

SEARCHING FOR NON GAUSSIAN SIGNALS IN THE BOOMERANG 2003 CMB MAPS

G. DE TROIA^{1,2}, P.A.R. ADE⁴, J.J. BOCK^{5,15}, J.R. BOND⁶, J. BORRILL^{7,17}, A. BOSCALERI⁸, P. CABELLA²¹, C.R. CONTALDI^{6,16}, B.P. CRILL⁹, P. DE BERNARDIS², G. DE GASPERIS¹, A. DE OLIVEIRA-COSTA¹³, G. DI STEFANO¹², P. G. FERREIRA²¹, E. HIVON¹¹, A.H. JAFFE¹⁶, T.S. KISNER^{7,17}, M. KUNZ²², W.C. JONES^{5,15}, A.E. LANGE¹⁵, M. LIGUORI²⁴, S. MASI², S. MATARRESE²³, P.D. MAUSKOPF⁴, C.J. MAC TAVISH⁶, A. MELCHIORRI^{2,18}, T.E. MONTROY²⁸, P. NATOLI^{1,19}, C.B. NETTERFIELD¹⁴, E. PASCALE¹⁴, F. PIACENTINI^{2,25}, D. POGOSYAN²⁰, G. POLENTA², S. PRUNET¹¹, S. RICCIARDI^{2,26}, G. ROMEO¹², J.E. RUHL³, P. SANTINI², M. TEGMARK¹³, M. VENEZIANI^{2,27}, AND N. VITTORIO^{1,19}.

Draft version February 1, 2008

ABSTRACT

We analyze the BOOMERanG 2003 (B03) 145 GHz temperature map to constrain the amplitude of a non Gaussian, primordial contribution to CMB fluctuations. We perform a pixel space analysis restricted to a portion of the map chosen in view of high sensitivity, very low foreground contamination and tight control of systematic effects. We set up an estimator based on the three Minkowski functionals which relies on high quality simulated data, including non Gaussian CMB maps. We find good agreement with the Gaussian hypothesis and derive the first limits based on BOOMERanG data for the non linear coupling parameter f_{NL} as $-300 < f_{\text{NL}} < 650$ at 68% CL and $-800 < f_{\text{NL}} < 1050$ at 95% CL.

Subject headings: cosmology: cosmic microwave background

1. INTRODUCTION

While cosmology is entering its precision era, the target of experiments aimed at the Cosmic Microwave Background (CMB) is shifting towards weak signals, e.g. polarization, the SZ effect and non Gaussian (NG) features. Detection of NG signals can be of significant help in constraining the mechanisms that explain the genera-

tion of cosmological perturbations. Provided that systematic effects will not degrade high sensitivity CMB mapping, present and future experiments could in principle be sensitive to non linearities due to second order effects in perturbation theory (Bartolo et al. 2004). This signal is usually parametrized by a non linear coupling factor f_{NL} that controls the level of a quadratic contribution to the primordial gravitational potential Φ (Komatsu and Spergel 2001):

$$\Phi(\mathbf{x}) = \Phi_G(\mathbf{x}) + f_{\text{NL}} [\Phi_G(\mathbf{x})^2 - \langle \Phi_G(\mathbf{x})^2 \rangle] \quad (1)$$

where Φ_G is a zero mean, Gaussian random field.

Several groups have reported NG constraints on CMB data. All suborbital efforts to date have found no significant deviation from Gaussianity in the CMB field: MAXIMA-1 reported $|f_{\text{NL}}| < 950$ at 1σ (Santos et al. 2003; Wu et al. 2001), while VSA found an upper limit of 5400 at 2σ (Smith et al. 2004); Archeops has recently improved their limits to $-800 < f_{\text{NL}} < 1100$ (2σ), although their analysis is based on assumptions only valid for the large angular scales dominated by the Sachs-Wolfe effect (Curto et al. 2006). The BOOMERanG 1998 dataset has also been tested for Gaussianity, both in pixel (Polenta et al. 2002) and in Fourier (De Troia et al. 2003) space, finding no trace of NG signals. However, BOOMERanG has set no f_{NL} limit so far. One of the purposes of this paper is to provide such limits with the analysis of the new 2003 data. The limits presented here are more stringent than those found by any suborbital experiment to date, properly accounting for sub-horizon angular scales.

The WMAP team constrained f_{NL} to be $-54 < f_{\text{NL}} < 114$ (Spergel et al. 2006). Using an improved version of the WMAP team estimator Creminelli et al. (2007) set the most stringent limits to date at $-36 < f_{\text{NL}} < 100$. Thus the f_{NL} analysis does not show any departure from Gaussianity in WMAP data. However, some authors have looked at general deviations from Gaussianity (i.e. not based on any specific parametrization of NG) and claimed highly-significant detection of NG features in

¹ Dip. Fisica, Università Tor Vergata, Roma, Italy
² Dip. Fisica, Università La Sapienza, Roma, Italy
³ Physics Department, Case Western Reserve University, Cleveland, OH, USA
⁴ Dept. of Physics and Astronomy, Cardiff University, Cardiff CF24 3YB, Wales, UK
⁵ Jet Propulsion Laboratory, Pasadena, CA, USA
⁶ Canadian Institute for Theoretical Astrophysics, University of Toronto, Toronto, Ontario, Canada
⁷ Computational Research Division, Lawrence Berkeley National Laboratory, Berkeley, CA, USA
⁸ IFAC-CNR, Firenze, Italy
⁹ IPAC, California Institute of Technology, Pasadena, CA, USA
¹⁰ Institut d'Astrophysique, Paris, France
¹¹ Istituto Nazionale di Geofisica e Vulcanologia, Roma, Italy
¹² Dept. of Physics, Massachusetts Institute of Technology, Cambridge, MA, USA
¹³ Physics Department, University of Toronto, Toronto, Ontario, Canada
¹⁴ Observational Cosmology, California Institute of Technology, Pasadena, CA, USA
¹⁵ Theoretical Physics Group, Imperial College, London, UK
¹⁶ Space Sciences Laboratory, UC Berkeley, CA, USA
¹⁷ INFN, Sezione di Roma 1, Roma, Italy
¹⁸ INFN, Sezione di Tor Vergata, Roma, Italy
¹⁹ Dept. of Physics, University of Alberta, Edmonton, AB, Canada
²⁰ Astrophysics, University of Oxford, Keble Road, Oxford OX1 3RH, UK
²¹ Département de Physique Théorique, Université de Genève, Switzerland
²² Dipartimento di Fisica G. Galilei, Università di Padova and INFN, Sezione di Padova, Italy
²³ Department of Applied Mathematics and Theoretical Physics, University of Cambridge, UK
²⁴ European Space Astronomy Centre (ESAC), European Space Agency, Madrid, Spain
²⁵ INAF- Osservatorio Astronomico di Padova, Italy
²⁶ APC, 10 rue Alice Domon et Lonie Duquet, 75, Paris Cedex 13
²⁷ Sierra Lobo, Inc. 11401 Hoover Rd. Milan, OH 44846, USA
²⁸

the WMAP maps (Copi et al. 2004; Vielva et al. 2004; Cruz et al. 2006).

In this paper we perform a pixel space analysis of the B03 temperature (T) data set, using the observed field’s moments and Minkowski functionals (MFs) to build Gaussianity tests. We assess the statistical significance of our results comparing the data to a set of highly realistic, Gaussian Monte Carlo (MC) simulated maps. In order to constrain f_{NL} , we build a goodness of fit statistics based on MFs and calibrated against a set of NG CMB maps, that are generated according to the algorithm set forth in (Liguori et al. 2003).

The plan of this letter is as follows: in section 2 we briefly describe the B03 experiment, the dataset it has produced and our simulation pipeline. In section 3 we compute the map’s moments and MFs of the data and compare results against Gaussian MC simulated maps. Then we derive constraints for f_{NL} . Finally, in section 4 we draw our main conclusions.

2. THE BOOMERANG 2003 DATASET

The balloon borne B03 experiment has been flown from Antarctica in 2003. It gathered data for 14 days in three frequency bands, centered at 145, 245 and 345 GHz. Here we restrict ourselves to the 145 GHz data that are most sensitive to CMB fluctuations. These have been obtained with polarization sensitive bolometers (PSB). The analysis of the dataset has produced high quality maps of the southern sky that have been conveniently divided in three regions: a “deep” (in terms of integration time) survey region (~ 90 square degrees) and a “shallow” survey region (~ 750 square degrees), both at high Galactic latitudes, as well as a region of ~ 300 square degrees across the Galactic plane. The deep region is completely embedded in the shallow region. Here we only consider a subset of the data that contains all of the deep region and part of the shallow, for a total of 693 square degrees (1.7% of the sky). The mask we use is square, 26 degrees in side, centered at about RA=82.6° and DEC=−44.2°, and excludes all detected point sources in the field. This region has been selected in view of high sensitivity CMB observation with low foreground contamination and was observed with a highly connected scanning strategy to keep systematics under control. We use the T data map reduced jointly from eight PSB at 145 GHz (Masi et al. 2005). In this region, the signal rms on 3.4’ pixels is $\sim 90 \mu\text{K}$ and instrumental noise has an rms of $\sim 20 \mu\text{K}$ in the deep region and of $\sim 90 \mu\text{K}$ in the shallow region. In harmonic space, binned estimates of the CMB angular power spectrum retain signal to noise > 1 well beyond $\ell \sim 1000$. One may compare these figures with WMAP: in the three year release, WMAP combined sensitivity in the region observed by B03 is $\sim 100 \mu\text{K}$ on 3.4’ pixels, close to WMAP’s mean pixel error. However, WMAP’s beams are broader than B03, so its ℓ space error is ~ 5 times larger than B03 at $\ell \simeq 1000$. On the other hand, B03 has not been devised to measure multipoles at $\ell \lesssim 50$. In this sense, our NG analysis probes angular scales complementary to those constrained by WMAP. While we do not consider here the Stokes Q and U polarization maps, our T map has been marginalized with respect to linear polarization. For a description of the instrument and the measured T and polarization maps see (Masi et al. 2005) and for the CMB

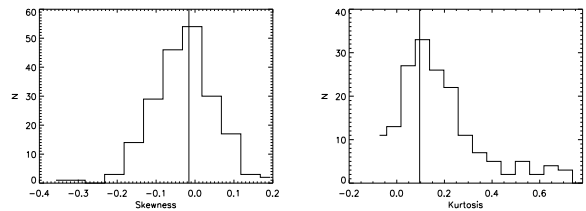


FIG. 1.— The left panel shows the distribution of S_3 estimator calculated from the 200 Gaussian MC maps. The S_3 value of the B03 data is represented by the vertical line. The right panel shows the same for S_4

TT, TE and EE power spectra see (Jones et al. 2006; Piacentini et al. 2006; Montroy et al. 2006).

To assess the robustness of our tests of Gaussianity we use a set of simulated MC maps that mimic the B03 data. To produce these, we follow the same steps performed when analysing real data. The Gaussian CMB sky signal is simulated from the power spectra that best fits the B03 data (MacTavish et al. 2006). This signal is smoothed according to the measured beam and synthesized into a pixelized sky map, using Healpix routines (Górski et al. 2005). Using the B03 scanning strategy, the signal map is projected onto 8 timestreams, one for each 145 GHz detector. Noise only timestreams are also produced, as Gaussian realizations of each detector’s noise power spectral density, estimated from the data accounting for cross talks among detectors. The timelines are reduced with the ROMA mapmaking code (Natoli et al. 2001; De Gasperis et al. 2005) replicating the actual flight pointing and transient flagging, to produce T, Q and U maps. With this procedure, we can simulate signal, noise and signal plus noise timestream.

To constrain f_{NL} we use MC simulations of NG CMB maps obtained from a primordial gravitational potential of the form given in eq. (1). These maps have been produced including first order CMB radiative transfer effects (Liguori et al. 2003). The power spectrum of the NG maps is identical to that of the Gaussian CMB simulations.

3. TESTS OF GAUSSIANITY AND CONSTRAINTS ON f_{NL}

Working at 6.8’ Healpix resolution ($N_{\text{side}} = 512$), we first compute the normalised skewness S_3 and kurtosis S_4 of our pixelized field T_i . These are obtained from the variance $\sigma^2 = 1/(N-1) \sum_i (T_i - \langle T \rangle)^2$ and from the third and the fourth moment $\mu_3 = \sum_i (T_i - \langle T \rangle)^3/N$ and $\mu_4 = \sum_i (T_i - \langle T \rangle)^4/N$, where N is the total number of pixels of the map and $\langle T \rangle = \sum_i T_i/N$ its mean. We have $S_3 = \mu_3/\sigma^3$, $S_4 = \mu_4/\sigma^4 - 3$. From the data we get $S_3 = -0.016$ and $S_4 = 0.096$. These values are plotted in Fig. 1 as a vertical line and compared to the empirical distribution as derived from the MC (signal plus noise) maps. From the latter we compute the probability $P(S_3^{\text{sim}} > S_3^{\text{data}}) = 58\%$ and $P(S_4^{\text{sim}} > S_4^{\text{data}}) = 77\%$. Hence, for these tests the data are compatible with the Gaussian hypothesis. The same tests are repeated after having degraded the map to 13.6’, finding similar results.

To analyse the map with MFs (Gott et al. 1990) we consider the excursion sets Q defined as the map’s subsets exceeding a given threshold ν : $Q(\nu) = \{T_i : (T_i - \langle T \rangle)/\sigma > \nu\}$. The three MFs measure the total area of the surviving regions of the map (M_0), their total con-

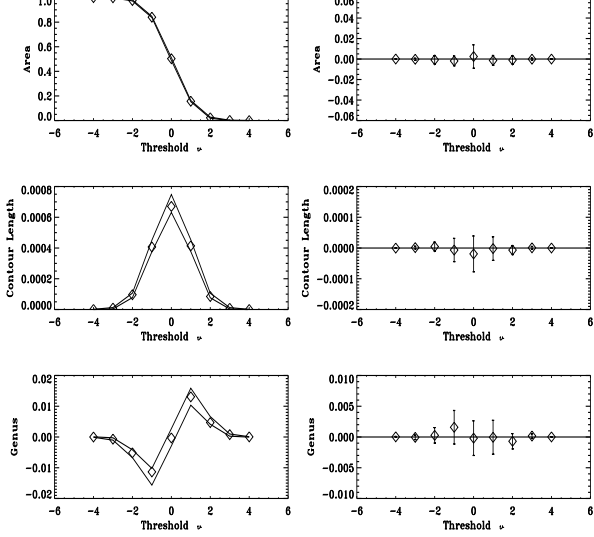


FIG. 2.— Left panels show the MFs estimated from the B03 data (diamonds) and the 2σ confidence limits from the 200 Gaussian MC maps. From top to bottom, the results correspond to the MFs M_0 , M_1 and M_2 , respectively. Right panels show the residuals between the MC mean and the data.

tour length (M_1), and the genus of the distribution which is related to the difference between the number of “hot” and “cold” regions (M_2). For a Gaussian field the expectation values of the functionals depend on a single parameter τ : $\langle M_0(\nu) \rangle = \frac{1}{2} \left[1 - \text{erf} \left(\frac{\nu}{\sqrt{2}} \right) \right]$, $\langle M_1(\nu) \rangle = \frac{\sqrt{\tau}}{8} \exp \left(-\frac{\nu^2}{2} \right)$, $\langle M_2(\nu) \rangle = \frac{\tau}{\sqrt{8\pi^3}} \nu \exp \left(-\frac{\nu^2}{2} \right)$. In the case of a pure CMB signal (no noise), τ is given by $\tau = \frac{1}{2} \sum_{\ell=1}^{\infty} (2\ell+1) \ell(\ell+1) C_\ell$ (Schmalzing and Górski 1998; Winitzki and Kosowsky 1998). Hence, M_1 and M_2 depend on the power spectrum C_ℓ . It is hence critical that the simulations reproduce the model C_ℓ ’s that best fits the data. We work in the flat sky limit, projecting our T values on the plane locally tangent to the map (Cabella et al. 2004). In Fig. 2 we plot MFs for the data and 2σ limits set by 200 Gaussian simulations, as well as the data residuals and their (again, 2σ) errors.

The functionals are computed at 9 thresholds evenly spaced between -4σ and $+4\sigma$.

Using the MC maps we can define a χ^2 statistic:

$$\chi_{B,i}^2 = \sum_{\nu\nu'} (M_i^B - \langle M_i^{sim} \rangle)_{\nu} C_{i,\nu\nu'}^{-1} (M_i^B - \langle M_i^{sim} \rangle)_{\nu'}. \quad (2)$$

Here M_i^B (M_i^{sim}) is any of the three MFs obtained from the data (simulations), $\langle \cdot \rangle$ is the mean value over MC realizations, and $C_{i,\nu\nu'} = \langle (M_{i,\nu} - \langle M_{i,\nu} \rangle)(M_{i,\nu'} - \langle M_{i,\nu'} \rangle) \rangle$ is a covariance matrix, estimated from an independent set of ~ 1000 Gaussian maps. In the first three panels of Fig. 3 we show χ_i^2 for each MF (vertical line), plotted along with the empirical distribution sampled via MC. We can define a “joint” estimator by grouping the M_i ’s in a single, 27 elements data vector $M_J \equiv \{M_0, M_1, M_2\}$ and defining a χ_B^2 as a trivial extension of Eq. 2. It is important that the covariance matrix built for the joint estimator correctly accounts for correlations among different functionals. However, we have found that in order to pin down to a stable level these off-block couplings, one requires a number realizations significantly higher than

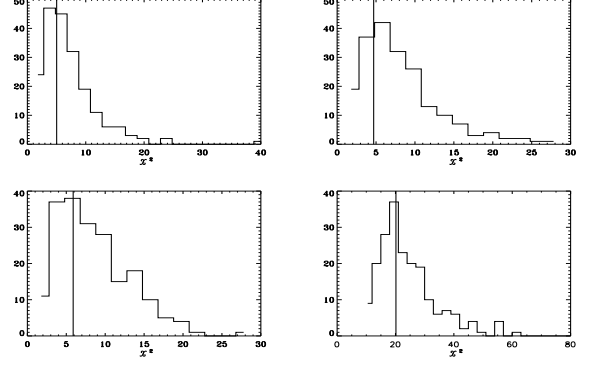


FIG. 3.— The χ_B^2 distribution (histogram) of MC simulated maps and data value (vertical line) for the MFs. Top: area and contour length. Bottom: genus and “joint” estimator (see text).

the ~ 1000 used throughout our analysis. The latter number cannot be realistically increased to desired level, because the GLS map making procedure is a demanding computational task, even for the supercomputers we have used. Fortunately, we have found that using white (instead of correlated) noise to estimate the covariance matrix has a negligible impact on the analysis. This finding can indeed be justified a posteriori, because the GLS map making procedure is very effective in suppressing noise correlations, that contribute very weakly to the estimator’s final covariance. The joint χ^2 of the data is displayed as the fourth panel in Fig. 3, along with the MC empirical distribution. The probability $P(\chi^2 > \chi_B^2)$ that a Gaussian map has a larger χ^2 than the B03 map is 76% for M_0 , 83% for M_1 , 76% for M_2 and 67% for the “joint” estimator. The values are fully consistent with the Gaussian hypothesis. We conclude that our pixel space analysis does not detect any sign of NG behavior in the B03 data.

We now want to constrain the quadratic coupling parameter f_{NL} defined in Eq. 1. To this purpose we simulate NG CMB realizations in the following way: firstly, we generate the Gaussian and NG part of the primordial potential defined by Eq. (1); then we convolve them with CMB first order radiation transfer functions to get the final CMB sky. In this way we produce 200 **G** (Gaussian) maps and 200 **NG** counterparts (each **G** map has a uniquely defined **NG** counterpart), so that for a given f_{NL} our (signal only) map is $\mathbf{G} + f_{NL} * \mathbf{NG}$. By adding noise maps, we can define MF estimators in the spirit of the section 3, with the difference that they are now functions of f_{NL} : $J_B(f_{NL}) = M_J^B - \langle M_J(f_{NL}) \rangle$ (we only consider the “joint” estimator in what follows). Consequently, we now define the data χ^2 as $\chi_B^2(f_{NL}) = J_B(f_{NL})^T \mathbf{C}^{-1} J_B(f_{NL})$. While in principle the covariance of the M_J ’s is a function of f_{NL} , this dependence is expected to be weak and is usually neglected (Komatsu et al. 2003). We have tested for this explicitly by using our NG simulations. We plot χ_B^2 as a function of f_{NL} in Fig. 4 (left panel). Goodness of fit analysis yields $-300 < f_{NL} < 650$ at 68% CL and $-800 < f_{NL} < 1050$ at 95%, with a best fit value (χ_B^2 at its minimum) of $f_{NL} = 200$. In order to cross check this result, we estimate a “frequentist” confidence interval for f_{NL} by sampling the empirical distribution of the M_J -based χ^2 , computed for $f_{NL} = 200$. The

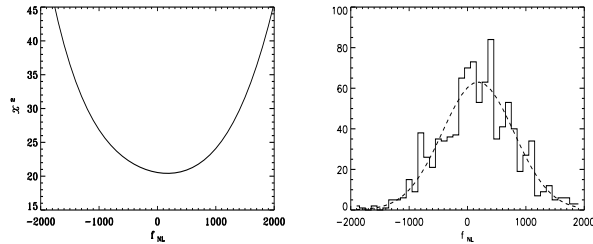


FIG. 4.— The left panel shows the B03 data χ^2 (χ_B^2 in the text) as a function of f_{NL} , while the panel on the right shows the empirical χ^2 distribution for NG maps ($f_{NL} = 200$), sampled using 1000 simulations

resulting histogram is displayed in the right panel of Fig.4. This analysis shows that we should expect to constrain $|f_{NL}| \lesssim 1000$ at 95%, thus suggesting that our limits derived through goodness of fit analysis are consistent. One may consider what limits on f_{NL} would be derived if we use, in place of MFs, the map’s skewness and kurtosis defined in Sect. 3 as elements of a two dimensional data vector. We thus repeated our goodness of fit analysis using these statistics and found weaker limits: $-950 < f_{NL} < 1350$ at 68% CL ($-1400 < f_{NL} < 1800$ at 95% CL). Even so, it is quite remarkable that a crude 1-point pixel statistic degrades the final sensitivity only by a factor ~ 2 . Of course, in order to find “optimal” constraints one has to implement a more sophisticated analysis.

The B03 dataset is not expected to be noise dominated at the 6.8’ resolution employed in the analysis above. To

show that this is the case, we repeated all of our procedures for 13.6’, finding similar (though slightly weaker) constraints.

4. CONCLUSIONS

We analysed the B03 145 GHz T map in search of NG signals. We worked in pixel space at 6.8’ and 13.6’ Healpix resolution. We computed the skewness and kurtosis of the map, as well as its three MFs. We compared these estimates against a set of simulated Gaussian maps that have been reduced using the same analysis pipeline as real data, finding no evidence of NG behavior. To quantify the latter statement, we define goodness of fit statistics jointly based on all three MFs, showing that the probability for a Gaussian simulation to have a χ^2 larger than the data is $\sim 67\%$. Assuming a model for primordial fluctuations that predicts a quadratic perturbation to the gravitational potential, we set limits on the non linear coupling parameter f_{NL} as $-800 < f_{NL} < 1050$ at 95% CL ($-300 < f_{NL} < 650$ at 68% CL). These limits may be regarded as complementary to the constraints set by WMAP in view of the better signal to noise ratio at high resolution in the B03 field.

BOOMERanG was supported by CIAR, CSA and NERSC in Canada, ASI, University La Sapienza and PNRA in Italy, NASA and NSF in the US. We thank CASPUR and NERSC/LBL. We acknowledge the use of HEALPix.

REFERENCES

- Bartolo N., Komatsu E., Matarrese S., & Riotto A., Phys. Rept., 402, 103, 2004
 Komatsu E., Spergel D.N., Phys.Rev., D63, 063002
 Komatsu E. et al.,Astrophys.J.Suppl. 148 (2003) 119-134, 2003
 Santos M.G., et al., MNRAS, 341, 623, 2003
 Wu J.H.P., et al., Phys.Rev.Lett. 87 (2001) 251303
 Smith S., et al., MNRAS, 352, 887, 2004
 Curto A., et al., astro-ph/0612148, submitted to A&A, 2006
 Polenta G., et. al., 2002, ApJ., 572 L27
 De Troia G., et. al., 2003 MNRAS, 343, 284
 Spergel D.N., et al., astro-ph/0603449, ApJ, in press
 Creminelli, P., et al., JCAP, 3, 5, 2007
 Copi C.J.,Huterer D.,Starkman G.D.,Phys.Rev.,D70, 043515, 2004
 Vielva P., et al., ApJ, 609, 22-34, 2004
 Cruz M., et al., MNRAS, 369, 57-67, 2006
 Liguori M., Matarrese S. and Moscardini L., ApJ., 597, 57, 2003
 Masi S. et al., astro-ph/0507509, submitted to A&A, 2005
 Jones W.C., et. al., Astrophys.J. 647, 823, 2006
 Montroy T.E., et al., Astrophys.J. 647, 813, 2006
 Piacentini F., et al., Astrophys.J. 647, 833, 2006
 MacTavish C.J., et al., Astrophys.J. 647, 799, 2006
 Natoli P., et al. , A&A, 371, 346, 2001
 de Gasperis G., et al., A&A, 436, 1159, 2005
 Gott J.R., et al., ApJ., 352, 1, 1990
 Cabella P., et al., Phys.Rev. D69, 063007, 2004
 Schmalzing J. and Górski K.M. , MNRAS, 297, 355, 1998
 Winitzki S. and Kosowsky A. , New Astron. 3, 75, 1998
 Górski K. M., et al., ApJ, 622, 759, 2005